A High-Power Millimeter-Wave Sheet Beam Free-Electron Laser Amplifier

Shiqiu Cheng, William W. Destler, *Fellow, IEEE,* Victor L. Granatstein, *Fellow, IEEE,* Thomas M. Antonsen, Jr., *Member, IEEE,* Baruch Levush, *Senior Member, IEEE,* John Rodgers, and Z. X. Zhang

***Abstract*—The results of experiments with a short period (9.6 mm) wiggler sheet electron beam (1.0 mm × 2.0 cm) millimeter-wave free electron laser (FEL) amplifier are presented. This FEL amplifier utilized a strong wiggler field for sheet beam confinement in the narrow beam dimension and an offset-pole side-focusing technique for the wide dimension beam confinement. The beam analysis herein includes finite emittance and space–charge effects. High-current beam propagation was achieved as a result of extensive analytical studies and experimental optimization. A design optimization resulted in a low sensitivity to structure errors and beam velocity spread, as well as a low required beam energy. A maximum gain of 24 dB was achieved with a 1-kW injected signal power at 86 GHz, a 450-kV beam voltage, 17-A beam current, 3.8-kG wiggler magnetic field, and a 74-period wiggler length. The maximum gain with a one-watt injected millimeter-wave power was observed to be over 30 dB. The lower gain at higher injection power level indicates that the device has approached saturation. The device was studied over a broad range of experimental parameters. The experimental results have a good agreement with expectations from a one-dimensional simulation code. The successful operation of this device has proven the feasibility of the original concept and demonstrated the advantages of the sheet beam FEL amplifier. The results of the studies will provide guidelines for the future developement of sheet beam FEL's and/or other kinds of sheet beam devices.**

I. Introduction

APPLICATIONS of free electron lasers (FEL's) in the microwave/millimeter-wave spectrum range from advanced particle accelerators [1], industrial material processing systems, long-range millimeter-wave radars [2], biomedical and molecular studies, and electron cyclotron resonance heating (ECRH) of plasmas for magnetic fusion. The International Thermonuclear Experimental Reactor (ITER) will require about 20 MW CW power in the frequency range of 100–300 GHz with a frequency tunability of a few percent for plasma initiation and for control of the tokamak current profile to minimize the occurrence of disruptive instabilities [3], [4]. Free electron laser amplifiers may become an attractive alternative to meet these requirements since they have the potential of producing a great deal of high power continuously over a wide tunable frequency range in a single unit. The sheet beam FEL amplifier of this research was initiated to meet these needs.

Manuscript received August 14, 1995; revised January 18, 1996. This work was supported by the U.S. Department of Energy.

The authors are with the Department of Electrical Engineering and Institute for Plasma Research, University of Maryland, College Park, MD 20742 USA (e-mail: scheng@glue.umd.edu).

Publisher Item Identifier S 0093-3813(96)04647-4.

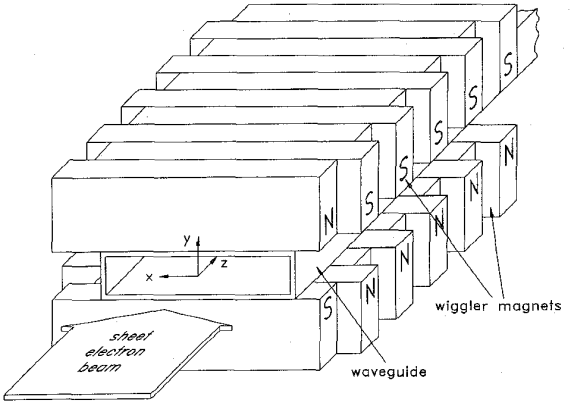

Fig. 1. An FEL structure utilizing sheet electron beam and planar wiggler.

Sheet electron beams have attractive features in a number of applications. In principle, beam current can be increased by increasing the width of the beam without a limitation on perveance. As opposed to solid beams or thin annular beams, sheet beams can also carry higher currents in small RF structures because of the higher space–charge current limits on flat sheet beams propagating between parallel conducting plates [5]. Sheet electron beams carrying high current can be very thin and thereby increase the beam/wave interaction efficiency by permitting strong coupling with a small-scale millimeter-wave circuit.

Fig. 1 shows a schematic of an FEL amplifier with a sheet electron beam. By utilizing a sheet beam, the gap in the center of the wiggler magnets can be reduced. An immediate benefit is the increased wiggler magnetic strength. In addition, total current can be increased without increasing current density by simply extending the wide dimension of the sheet beam. Associated with this thin sheet beam and a small wiggler gap can be a very short wiggler period, which results in a reduction of the required beam voltage compared with other FEL concepts for fusion applications [6], [7]. This can considerably reduce the size and cost of the high-power supplies required to drive such devices.

The objective of this research was to develop an initial working device embodying these features as a future multimegawatt millimeter-wave source for application in fusion

demonstration reactors. Earlier studies on sheet beam FEL's [8]–[22] paved the ground for the successful completion of this work. After an observation of a small amplification signal [17], an increase in the amplification gain was first achieved at 94 GHz as a result of increased propagated beam current and improved waveguide uniformity [18]. The high power experiment at 86 GHz employing the same hardware showed a much lower gain. The discrepancy between the achieved gain from these two experiments was then analyzed in terms of structure imperfection and electron beam quality, as well as device design parameters [20]. It was found that these factors favored operation at 94 GHz rather than 86 GHz. An improved design, which reduced the detrimental effect of the unavoidable structural errors, resulted in a high-gain high-power amplification and the saturation of the device. This paper details the design, analysis, and results.

II. Design Principles

Microwaves or millimeter-waves that participate in the interaction are usually confined inside a waveguide. The waveguide mode dispersion relation is described by

$$\omega^2 = (k_c^2 + k_z^2)c^2 \tag{1}$$

where c is the speed of light and k_c is the cutoff wavenumber. In a rectangular waveguide of cross section $a \times b$, the cutoff wavenumber for a TE_{mn} or TM_{mn} mode is given by

$$k_c = \left[\left(\frac{m\pi}{a}\right)^2 + \left(\frac{n\pi}{b}\right)^2\right]^{1/2}. \tag{2}$$

The dispersion of an electron beam drifting inside a waveguide, in general, has fast and slow branches, called space–charge waves. In a sheet beam FEL amplifier, the low current density makes the space–charge effect modification to the dispersion negligible. However, the dispersion of an electron beam in an FEL is modified by the spatially periodic magnetic field of a wiggler. This modification of the beam dispersion provides a means to couple the electromagnetic field with the electron beam, which is the basic idea of FEL's.

The modified beam dispersion is described as

$$\omega \approx (k_w + k_z)\beta_z c \tag{3}$$

where

$$k_w = \frac{2\pi}{\lambda_w}. \tag{4}$$

λ_w is the period of wiggler and

$$\beta_z = \left(1 - \frac{1}{\gamma_z^2}\right)^{1/2} \tag{5}$$

is the z-direction velocity normalized to the speed of light.

An FEL amplifier operates at the injected signal frequency if we do not consider the slight frequency shift caused by the time variation of beam parameters [23]. The dispersion relations determine the relationship between the resonant axial beam energy, the wiggler parameters, and the amplifier waveguide geometry. By combining the dispersion relations, the required z velocity at the resonance condition can be obtained as

$$\beta_{zr} \approx \frac{\omega/c}{k_w + \sqrt{(\omega/c)^2 - k_c^2}}. \tag{6}$$

These dispersion relations are the basic equations for the design and analysis of FEL's. From (6), the advantage of using a small period wiggler is obvious, i.e., it results in a reduction in the required beam energy.

Beam quality and structural uniformity have effects on operation of an FEL device. Beam energy spread affects γ_z of the beam. Structure errors affect the γ_{zr} required for resonance. In essence, any of these imperfections, alone or together, affect the energy detuning $\gamma_z - \gamma_{zr}$. A 5% error in $\Delta\gamma_z/\gamma_z$ when γ_z is about two implies an equivalent beam voltage spread of approximately 50 kV. With such a voltage spread, the FEL amplifier can be switched from amplification to absorption. If the beam velocity spread or structure imperfection causes only a several kilovolt detuning voltage change, this effect may be negligible.

Assuming waveguide dimension and wiggler period to have constant errors throughout the waveguide along the wiggler length, manipulations of the dispersion relations result in

$$\frac{\Delta\gamma_{zr}}{\gamma_{zr}} = \left[\frac{\Delta\omega_c}{\omega\sqrt{(\omega/\omega_c)^2 - 1}} - \frac{\Delta k_w c}{\omega}\right]\gamma_{zr}^2\beta_{zr}^3. \tag{7}$$

The uniform errors approximation greatly simplifies the analyses, which lead to important conclusions, although the actual errors are randomly distributed. For given errors in waveguide dimension and wiggler period, their effect on $\Delta\gamma_{zr}/\gamma_{zr}$ can be reduced by proper choice of the amplifier design parameters. Preferred device operation regime is that the beam line is tangential to the waveguide mode curve. Operation of an FEL amplifier around this region can reduce not only the required beam energy, but also the effect of the unavoidable fabrication errors [24].

The effect of wiggler field amplitude error on FEL amplification is small. The following relation holds for a planar wiggler FEL:

$$\gamma = \gamma_z(1 + \tfrac{1}{2}a_w^2)^{1/2} \tag{8}$$

where

$$a_w = \frac{eB_w}{mck_w}.$$

A change in wiggler field amplitude can result in a change in axial energy of the beam electrons

$$\frac{\Delta\gamma_z}{\gamma_z} = -\frac{a_w^2}{2 + a_w^2}\left(\frac{\Delta B_w}{B_w}\right). \tag{9}$$

For a 3% field amplitude error at $a_w = 0.3$, the $\Delta\gamma_z/\gamma_z$ is less than 0.2%.

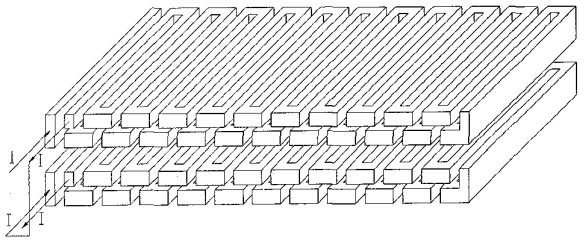

Fig. 2. Schematic of the electromagnet planar wiggler.

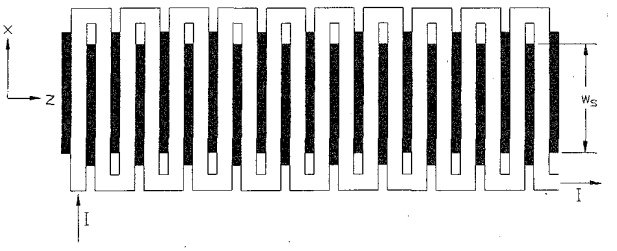

Fig. 3. Illustration of the offset pole technique for the wide dimension electron beam confinement.

III. Wiggler

The wiggler used in the experiment is a pulsed electromagnet. The planar wiggler structure is compatible with sheet electron beams and is relatively easy to fabricate. Fig. 2 shows a schematic. A combination of wiggler sections constitutes the whole wiggler. There are four pieces in each section, two on the top and two at the bottom, with the amplifier waveguide inserted in the channel between the top and bottom components. The current on the sides of each piece runs in the opposite direction. Such an arrangement effectively cancels the spurious magnetic field, generated by the edge current, inside the FEL interaction region.

The planar wiggler field has been derived earlier in [8]. The fundamental harmonic field utilized in the sheet beam FEL amplifier can be expressed as

$$B_y(y,z) = B_w \cosh(k_w y)\sin(k_w z) \tag{10}$$

$$B_z(y,z) = B_w \sinh(k_w y)\cos(k_w z). \tag{11}$$

For improved beam propagation and beam matching, a proper tapering of the wiggler field profile at the beam entrance from zero to B_w is very important. The wiggler entrance taper profile employed in the experiments has the form

$$B_w(z) = \begin{cases} B_w \sin^2\left(\dfrac{k_w z}{4N_{\rm tap}}\right) & 0 \le z \le N_{\rm tap}\lambda_w \\ B_w & N_{\rm tap}\lambda_w < z \end{cases} \tag{12}$$

where $N_{\rm tap}$ is the number of tapered periods. This tapering was achieved experimentally by a combination of gradually reducing the short current and gradually increasing the number of ferrite magnetic pieces.

The wide dimension beam confinement is provided by the offset pole technique, which is illustrated in Fig. 3. Taking the offset-pole magnetic field into account, the total magnetic field is the contributions from the uniform wiggler and the offset-pole pieces, i.e.,

$$\boldsymbol{B}_{\rm total} = \boldsymbol{B}_w + \boldsymbol{B}_{\rm off}. \tag{13}$$

Sheet beam propagation inside such a field is next analyzed and the experimental measurement results are presented.

IV. Wiggler-Focused Sheet Beam Propagation

A rectangular sheet electron beam is actually not stable if one considers the electrons at the corner edges [25]. However, a real sheet beam can be approximated by a beam of elliptical cross section and large aspect ratio. The transport of elliptical beams has been studied using a self-consistent theory assuming a uniform charge distribution, which is a result of an assumed K–V distribution [26]. The uniform charge density is expressed as

$$\rho_o(z) = \frac{I}{\pi \overline{v}_z X(z) Y(z)} \tag{14}$$

where X and Y represent beam envelopes in the transverse cross section. The components of the space–charge electric field are

$$E_x = \frac{I}{\pi\epsilon_o \overline{v}_z}\frac{x}{X(X+Y)} \tag{15}$$

$$E_y = \frac{I}{\pi\epsilon_o \overline{v}_z}\frac{y}{Y(X+Y)}. \tag{16}$$

ϵ_o is the permittivity of vacuum. Similar expressions can be obtained for the magnetic self-field. When emittance is taken into account in addition to the space–charge and self magnetic fields, the envelope equations (paraxial approximation) become

$$X'' + \kappa_x X - \frac{2K}{X+Y} - \frac{\epsilon_x^2}{X^3} = 0 \tag{17}$$

$$Y'' + \frac{\Omega_\beta^2}{\overline{v}_z^2} Y - \frac{2K}{X+Y} - \frac{\epsilon_y^2}{Y^3} = 0. \tag{18}$$

Here

$$\Omega_\beta = \frac{eB_w}{\sqrt{2}\gamma m}$$

$$K = \frac{eI}{2\pi\epsilon_o m c^3 \beta_z^3 \gamma \gamma_z^2}$$

is the generalized perveance of the beam, and κ_x represents the external focusing force along the x direction such as the deflection force resulting from wiggler offset-pole pieces. In the above envelope equations, the second terms represent the wiggler-focusing force, the third terms space–charge and self magnetic field effects, and the last the emittance terms. ϵ_x and ϵ_y are the effective emittances of the sheet electron beam [22] in the x and y dimensions, respectively.

Using an ideal model [25], the y-component of the side-focusing field can be approximated as

$$B_{y,\rm off} = \frac{B_s}{2\pi}\left[\tan^{-1}\left(\frac{w_s/2+x}{b_m/2-y}\right) - \tan^{-1}\left(\frac{w_s/2-x}{b_m/2-y}\right) + \tan^{-1}\left(\frac{w_s/2+x}{b_m/2+y}\right) - \tan^{-1}\left(\frac{w_s/2-x}{b_m/2+y}\right)\right] \tag{19}$$

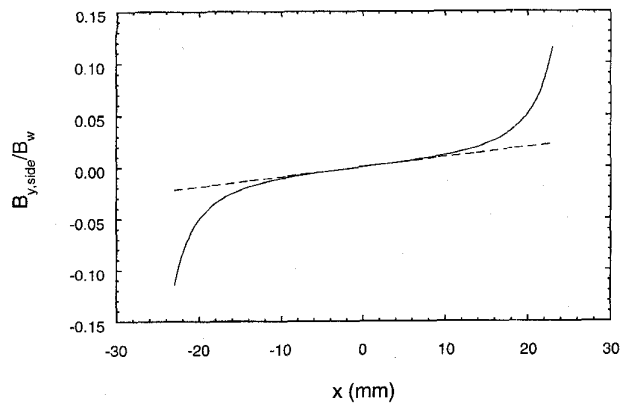

Fig. 4. Side-focusing field, analytic (solid) and approximated (dashed). $w_s = 5.0\,\text{cm}, b_m = 3.8\,\text{mm}, y = 0$ for the analytic plot.

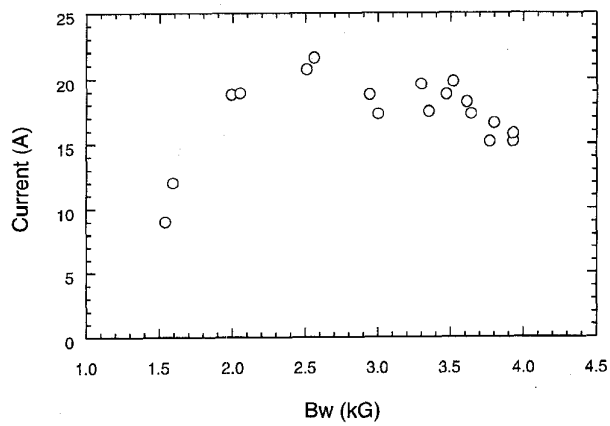

Fig. 5. Propagated beam current through the 74-period wiggler. $v_{\text{beam}} = 450 \pm 4\,\text{kV}$. The waveguide narrow dimension $b = 3.2\,\text{mm}$.

where w_s has been illustrated in Fig. 3, b_m is the wiggler gap size, and B_s is the limit of $|B_{y,\text{off}}|$ when $x \to \pm\infty$. This result can be approximated by using Taylor-expansion, keeping only the terms up to the first order, yielding

$$\begin{aligned}&\tan^{-1}\left(\frac{w_s/2+x}{b_m/2-y}\right)-\tan^{-1}\left(\frac{w_s/2-x}{b_m/2-y}\right)\\&+\tan^{-1}\left(\frac{w_s/2+x}{b_m/2+y}\right)-\tan^{-1}\left(\frac{w_s/2-x}{b_m/2+y}\right)\\&\approx\frac{8b_mx}{b_m^2+w_s^2}\equiv 4\pi gx\end{aligned}\tag{20}$$

where g is a geometric factor only depending on the geometry. Proper design of the offset pole structure is required for balancing a sheet electron beam according to its property. The desired factor g can be obtained by adjusting b_m and w_s. Fig. 4 illustrates a profile of the side-focusing field with this linear approximation. From a practical point of view, a stronger side-focusing force is desirable. The approximation gives a weaker field off the axis than that obtained from the analytical expression. However, when wiggler lamination saturation is considered, the actual side-focusing field profile will be flattened to some extent, therefore approaching the approximated result.

The period-averaged side-focusing force can be calculated using the above approximation, resulting in

$$\kappa_x = \frac{g\Omega_\beta}{\overline{v}_z}.\tag{21}$$

The matched beam envelopes, for which $X'' = 0$ and $Y'' = 0$, are then determined by

$$\frac{g\Omega_\beta}{\overline{v}_z}x_m-\frac{2K}{x_m+y_m}-\frac{\epsilon_x^2}{x_m^3}=0\tag{22}$$

$$\frac{\Omega_\beta^2}{\overline{v}_z^2}y_m-\frac{2K}{x_m+y_m}-\frac{\epsilon_y^2}{y_m^3}=0.\tag{23}$$

In the case $B_w = 3.8\,\text{kG}, V_{\text{beam}} = 450\,\text{kV}, \lambda_w = 9.6\,\text{mm}, I = 20\,\text{A}, \epsilon_{n,x} = 1900$ mm-mrad, and $\epsilon_{n,y} = 70$ mm-mrad, it gives a result of $x_m = 11.3\,\text{mm}, y_m = 0.67\,\text{mm}$ for the matched beam. $\epsilon_n = \beta\gamma\epsilon$ is the normalized effective emittance. The emittance values used in this numerical example are measured results [22]. Other parameters correspond to the saturation experiment that will be presented in the next section. For an unmatched beam with a small mismatch, the envelope equations can be approximately solved analytically by keeping only the zeroth- and first-order approximation terms and utilizing the relations for a matched beam. The result shows a scalloping envelope.

Propagated beam current was measured using a Faraday cup, located at the down-stream end of the amplifier waveguide. The measured wiggler entrance taper profile is very close to $\sin^2(k_w z/4N_{\text{tap}})$ with $N_{\text{tap}} = 4$ for a B_w in the vicinity of 3.5 kG. Fig. 5 shows the result of beam propagation through a waveguide $3.2\,\text{mm} \times 4.0\,\text{cm}$ in cross section and 74 wiggler periods in length. The experimental beam voltages were close to the required FEL amplifier operating voltage.

An entrance taper profile can only be optimized for a specific wiggler discharge (energizing) current, i.e., for a specific peak wiggler field B_w. Beam propagation also depends on the operating voltage, even for a fixed wiggler entrance taper. This dependence should be very weak for a sine squared taper profile. However, an optimized entrance taper is very difficult to obtain in reality. Therefore, this voltage dependence can be significant, as has been observed in the experiments.

V. Amplification Experiments

A schematic of the experimental setup is shown in Fig. 6. An explosive field emission diode [21] generates sheet electron beams for the FEL amplifier. Tungsten graphite was used as the cathode material. A charged capacitor bank pulse drives the electromagnetic wiggler. The propagated beam current is monitored using a calibrated Rogowski coil located at the down-stream end of the amplifier waveguide. An extended interaction oscillator (EIO) generates millimeter-wave and provides input RF power for the amplifier. It is capable of producing 1.7 kW of peak power at 86 GHz with a duration of up to 2 μs. An electroformed waveguide taper converts

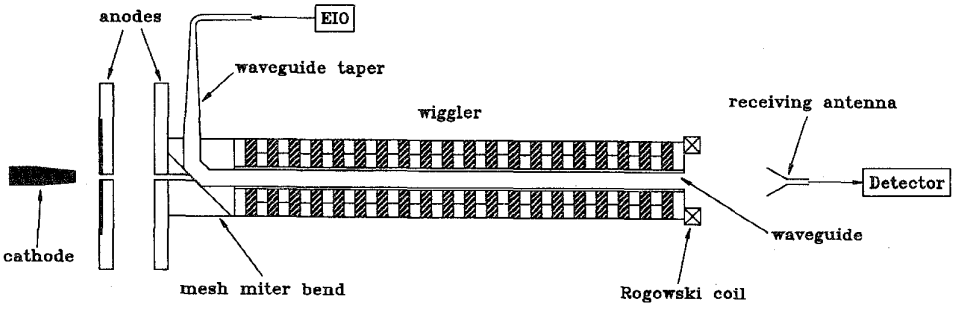

Fig. 6. Schematic of sheet beam FEL amplifier experiments.

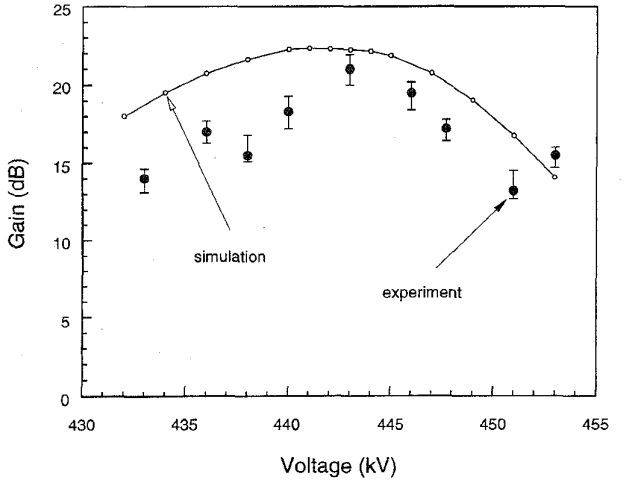

Fig. 7. A plot of gain versus beam voltage with a narrowly defined wiggler field range around 3.5 kG. Beam current for the simulation is 16 A while experimental beam currents were 16–17.6 A. The error in experimental beam voltage is ±2 kV.

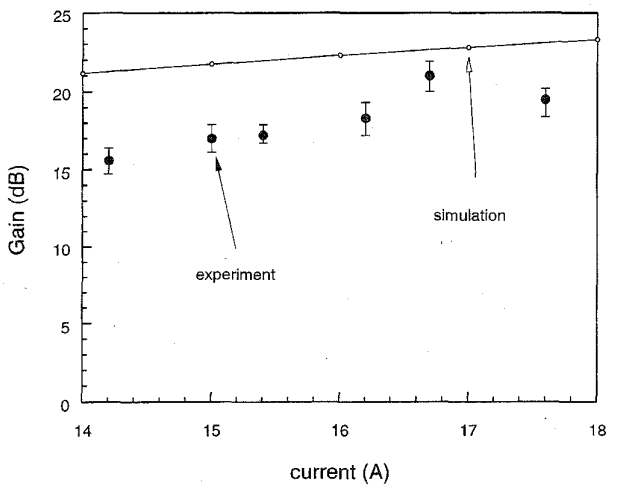

Fig. 8. A plot of gain versus beam current with a narrowly defined wiggler field range around 3.5 kG. Beam voltage has been optimized for each point in the simulation.

the RF output of the EIO from the fundamental $TE_{10}^{\square}$ mode of the standard WR-10 waveguide (2.54 mm by 1.27 mm inner dimensions) to the $TE_{01}^{\square}$ mode of the FEL amplifier waveguide. The amplifier waveguide has an interior cross-sectional dimensions of 3.2 mm by 4.0 cm. The operating parameters were chosen in such a way that the dispersion line of the electron beam is almost tangential to the waveguide mode dispersion curve. The electron beam and RF signal are coupled through a 45° mesh miter bend acting as a beam/wave coupler, which has about 90% reflectivity for the RF power and 90% transparency for the electron beam current. The amplified RF signal radiates through the open end of the amplifier waveguide and is sampled in the far radiation field region using a horn antenna. The antenna is oriented in such a way that it can only receive radiation with its electric field parallel to the wide dimension of the rectangular amplifier waveguide. When such an orientation was rotated 90° around the axis of the FEL amplifier system, there was no signal observed.

Several attenuators were inserted between the pickup horn antenna and the detector to reduce the detected millimeter-wave signals to an appropriate level so that the detector would be neither saturated nor damaged. In higher gain measurements, two channels of the digital oscilloscope were set at different scales to record respective input and amplified signals simultaneously. The detector was carefully calibrated over a wide range of detection power levels.

Amplification or absorption occured under certain beam voltage, beam current, and wiggler magnetic field conditions. No amplified signal was observed if either the wiggler magnetic field or the EIO source was turned off. A maximum gain of 24 dB at 1 kW input power and a maximum gain of over 30 dB at 1 W input power have been achieved.

A plot of gain versus beam voltage with a 3.5-kG peak wiggler magnetic field and a narrowly defined beam current range is shown in Fig. 7. Open circles are the numerical results from a one-dimensional (1-D) simulation code [18], [19]. Gain versus beam current for a narrow range of wiggler field is plotted in Fig. 8. Voltage has been optimized for each operating point in the simulation. Figs. 9 and 10 are the plots corresponding to a wiggler field around 3.8 kG. Fig. 11 shows a plot of gain versus peak wiggler field for a narrow range of beam current. As has been discussed in the previous section, the wiggler entrance taper profile was adjusted only for a particular energizing current of the wiggler magnets. Good beam matching was only expected in that particular case. This may be the reason of the lower gain than the simulation at lower wiggler magnetic field. In addition, since an optimized wiggler entrance taper was difficult to achieve in practice,

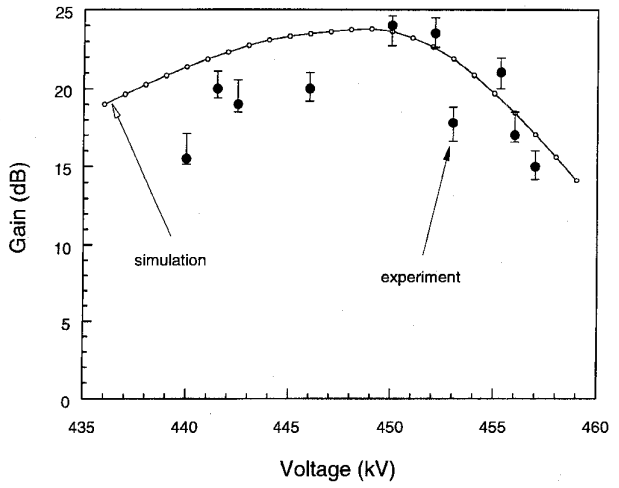

Fig. 9. A plot of gain versus beam voltage with wiggler magnetic field around 3.8 kG. Beam current is 17 A for the simulation while experimentally measured currents were 15.3–17.3 A. $\Delta V_{\exp} = \pm 2$ kV.

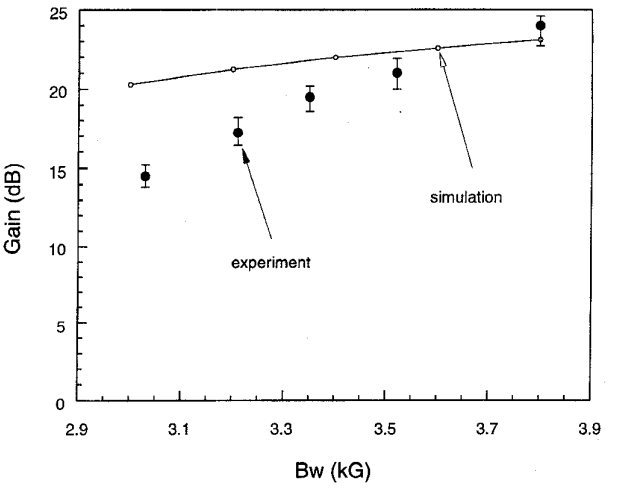

Fig. 11. A plot of gain versus wiggler magnetic field amplitude. Experimentally measured beam currents were 16–17.5 A, beam current for the simulation is 16 A.

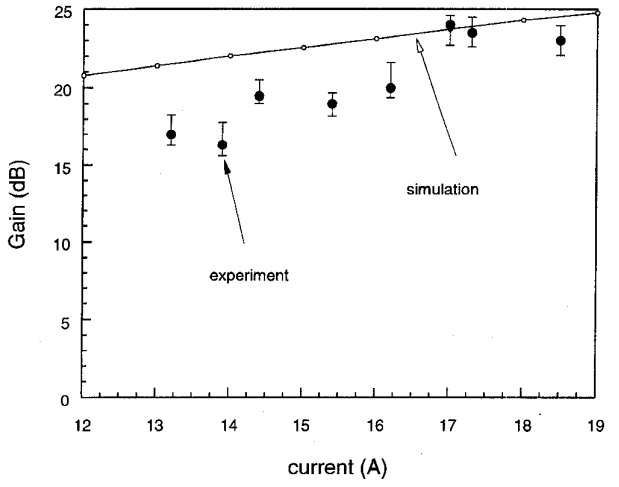

Fig. 10. A plot of gain versus beam current with wiggler field around 3.8 kG. Beam voltage has been optimized for each point in the simulation.

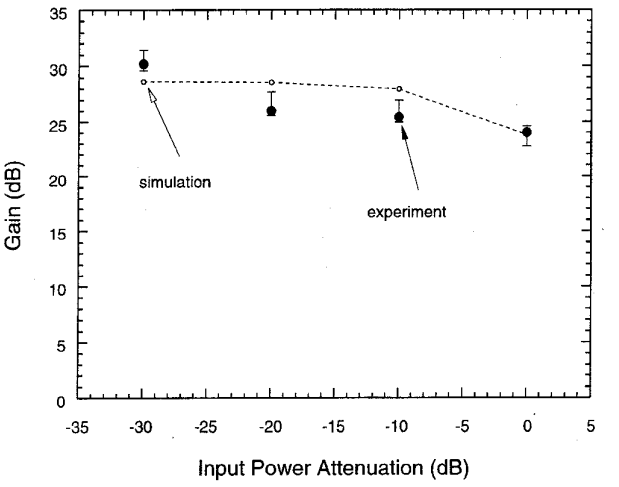

Fig. 12. A plot of gain versus input power level with wiggler field around 3.8 kG. Experimentally measured beam currents were 16–17.2 A. Current for the simulation is 17 A. $\overline{\theta} = 4°$.

beam propagation had certain dependence on the beam voltage and so had gain of the device. Gain versus input power level was also measured and is plotted in Fig. 12. The lower gain observed at higher RF input power levels indicates that the device is in saturation.

The model of the 1-D simulation code has been detailed in [18]. The only free parameter in the simulation is an angular momentum spread of the injected electron beam. This spread is assumed to have a Gaussian distribution with a characteristic spread $\overline{\theta}$. The numerical simulations shown in this paper used a $\overline{\theta} = 4°$. If a maximum wiggler period error of $\pm 3\%$ and a maximum waveguide narrow dimension error of ± 0.25 mm are assumed, (7) gives a maximum $|\Delta\gamma_{zr}|/\gamma_{zr}$ of about 7%. For the previous experiments [18], [20], the structural errors in the experiments were estimated to be $\pm 3\%$ for the wiggler period and ± 0.1 mm for the waveguide narrow dimension. According to the analysis here, the maximum $|\Delta\gamma_{zr}|/\gamma_{zr}$ is calculated to be up to 8% at 86 GHz or 6% at 94 GHz. Although the waveguide error is larger than that of the previous experiments, the effect on $\Delta\gamma_{zr}/\gamma_{zr}$ is smaller because of the proper choice of the operating point of the device.

VI. Conclusions and Future Developments

A novel millimeter-wave FEL amplifier utilizing a sheet electron beam and a small period planar wiggler has been experimentally studied over a broad range of parameters, including wiggler magnetic field, beam current, beam voltage, and RF input power.

The device approached saturation at a wiggler length of 71 cm with a gain of 24 dB at a 1 kW input power. This gain was achieved with only 450 kV beam voltage, 17 A beam current, and 3.8 kG wiggler magnetic field, and clearly demonstrates

the advantages of utilizing a sheet beam and a short period wiggler in an FEL amplifier.

Future developments will include design and construction of a thermionic electron gun and superconducting wiggler magnets for high-power operation, as well as a tapering of the wiggler structure and utilization of depressed-collector system for efficiency enhancement. A compact system for CW or high repetition rate operation calls for the development of a thermionic electron gun. Sheet beam electron guns have been developed to a lesser extent than have pencil beam or coaxial hollow beam configurations, although converting a pencil beam generated from a Pierce-type electron gun using a magnetic quadropole [27] can form a sheet electron beam. However, a greater effort should be made toward the design and development of electron guns to directly generate sheet (strip) beams. An FEL with a permanent magnet wiggler is rugged and compact, while an FEL with a superconducting wiggler will have a much higher saturation power. Efficiency is an important figure of merit for evaluating the potential application of a device. High-efficiency FEL's require high-quality electron beams. With a well-developed thermionic electron gun, efficiency enhancement issues will be well studied using different tapering schemes as appropriate for short-period wiggler FEL's. The addition of a single-stage or multi-stage depressed-collector system will further increase the overall efficiency of an FEL.

ACKNOWLEDGMENT

The authors acknowledge the engineering support from J. Pyle, D. Cohen, and K. Diller.

REFERENCES

[1] G. Bekefi, B. Chen, I. Mastovsky, P. Volfbeyn, I. Wilson, and W. Wuensch, "Experimental studies of a high gradient RF accelerating structure driven by a 33 GHz free electron laser amplifier," in *ICOPS'94*, Santa Fe, NM, June 6–8, 1994, *Abstracts 94CH3465-2,* vol. 2D10–11, p 114.

[2] N. C. Currie and C. E. Brown, *Principles and Applications of Millimeter-Wave Radar.* Dedham, MA: Artech House, 1987.

[3] R. W. Conn, V. A. Chuyanov, N. Inoue, and D. R. Sweetman, "The international thermonuclear experimental reactor," *Sci. Amer.,* vol. 266, pp. 103–110, Apr. 1992.

[4] K. Tomabechi, J. R. Gilleland, Yu. A. Sokolov, R. Toschi, and the ITER Team, "ITER conceptual design," *Nucl. Fusion,* vol. 31, pp. 1135–1224, 1991.

[5] G. Providakes, J. A. Nation, and M. E. Read, "Microwave generation using sheet relativistic electron beams," *IEEE Trans. Microwave Theory Tech.,* vol. MTT-25, pp. 563–566, 1977.

[6] P. W. Van Amersfoort, R. J. Bakker, J. B. Bekkers, R. W. B. Best, R. Van Buuren, P. F. M. Delmee, B. Faatz, C. A. J. van der Geer, D. A. Jaroszynski, P. Manintveld, W. J. Mastop, B. J. H. Meddens, A. F. G. van der Meer, J. P. Nijman, D. Oepts, J. Pluygers, and M. J. van der Wiel, "First lasing with FELIX," *Nucl. Instrum. Method Phys. Res. A,* vol. 318, pp. 42–46, 1992.

[7] A. L. Throop, R. A. Jong, S. L. Allen, D. P. Atkinson, J. C. Clark, B. Felker, S. W. Ferguson, M. A. Makowski, W. E. Nexsen, B. W. Rice, B. W. Stallard, and W. C. Turner, "140 GHz microwave FEL experiments using ELF-II," *Nucl. Instrum. Method Phys. Res. A,* vol. 296, pp. 41–49, 1990.

[8] W. W. Destler, V. L. Granatstein, I. D. Mayergoyz, and Z. Segalov, "Near-millimeter free electron laser designs based on measured characteristics of small-period electromagnet wigglers," *J. Appl. Phys.,* vol. 60, pp. 521–528, 1986.

[9] T. M. Antonsen, Jr. and P. E. Latham, "Linear theory of a sheet beam free electron laser," *Phys. Fluids,* vol. 31, pp. 3379–3386, 1988.

[10] V. L. Granatstein, T. M. Antonsen, Jr., J. H. Booske, W. W. Destler, P. E. Latham, B. Levush, I. D. Mayergoyz, D. J. Radack, Z. Segalov, and A. Serbeto, "Near-millimeter free electron lasers with small period wigglers and sheet electron beams," *Nucl. Instrum. Method Phys. Res. A,* vol. 272, pp. 110–116, 1988.

[11] D. J. Radack, J. H. Booske, Y. Carmel, and W. W. Destler, "Wiggler focused relativistic sheet beam propagation in a planar free-electron laser configuration," *Appl. Phys. Lett.,* vol. 55, pp. 2069–2071, 1989.

[12] J. H. Booske, D. J. Radack, T. M. Antonsen, Jr., S. W. Bidwell, Y. Carmel, W. W. Destler, H. P. Freund, V. L. Granatstein, P. E. Latham, B. Levush, I. D. Mayergoyz, and A. Serbeto, "Design of high-average-power near-millimeter free electron laser oscillators using short-period wigglers and sheet electron beam," *IEEE Trans. Plasma Sci.,* vol. 18, pp. 399–415, 1990.

[13] S. W. Bidwell, Z. X. Zhang, T. M. Antonsen, Jr., W. W. Destler, V. L. Granatstein, B. Levush, J. Rodgers, and H. P. Freund, "Development of a high power millimeter wave free-electron laser amplifier," in *Beams92, Proc. 9th Int. Conf. High-Power Particle Beams,* 1992, pp. 1728–1733.

[14] V. L. Granatstein, W. W. Destler, S. W Bidwell, Z. X. Zhang, T. M. Antonsen, Jr., B. Levush, J. Rodgers, and Y. Carmel, "Experimental and numerical results on a millimeter-wave free electron laser amplifier," *Nucl. Instrum. Method Phys. Res. A,* vol. 331, pp. 122–125, 1993.

[15] J. H. Booske, W. W. Destler, Z. Segalov, D. J. Radack, E. T. Rosenbury, J. Rodgers, T. M. Antonsen, Jr., V. L. Granatstein, and I. D. Mayergoyz, "Propagation of wiggler focused relativistic sheet electron beams," *J. Appl. Phys.,* vol. 64, pp. 6–11, 1988.

[16] Z.-X. Zhang, V. L. Granatstein, W. W. Destler, S. W. Bidwell, J. Rodgers, S. Cheng, T. M. Antonsen, Jr., B. Levush, and D. J. Radack, "Experimental and numerical studies of sheet electron beam propagation through a planar wiggler magnet," *IEEE Trans. Plasma Sci.,* vol. 21, pp. 760–767, 1993.

[17] Z.-X. Zhang, W. W. Destler, V. L. Granatstein, T. M. Antonsen, Jr., B. Levush, J. Rodgers, and S. Cheng, "Experimental realization of millimeter-wave amplification by a sheet beam free electron laser," *Appl. Phys. Lett.,* vol. 64, pp. 1439–1441, 1994.

[18] W. W. Destler, S. Cheng, Z. X. Zhang, T. M. Antonsen, Jr., V. L. Granatstein, B. Levush, and J. Rodgers, "First operation of a wiggler-focused, sheet beam free electron laser amplifier," *Phys. Plasmas,* vol. 1, pp. 1708–1713, 1994.

[19] B. Levush, H. P. Freund, and T. M. Antonsen, Jr., "Tunability of tapered free electron lasers," *Nucl. Instrum. Meth. Phys. Res. A,* vol. 341, pp. 234–237, 1994.

[20] S. Cheng and W. W. Destler, "High power operation of a wiggler-focused sheet beam free electron laser amplifier," *Nucl. Instrum. Meth. Phys. Res. A,* vol. 358, pp. 200–203, 1995.

[21] S. Cheng, W. W. Destler, V. L. Granatstein, and J. Rodgers, "Generation of sheet electron beams for experiments on a wiggler-focused small period free electron laser amplifier," in *Beams 94, Proc. 10th Int. Conf. High Power Particle Beams,* vol. 2, pp. 523–526, 1994.

[22] S. Cheng and W. W. Destler, "Sheet beam emittance measurements by slit-pinhole method," to appear in *Nucl. Instrum. Meth. Phys. Res.*

[23] G. Bekefi, B. Chen, M. E. Conde, I. Mastovsky, K. Ricci, C. J. Taylor, and P. Volfbeyn, "Observations of frequency chirping and phase of a free electron laser amplifier," MIT Rep., Aug. 1993.

[24] S. Cheng, "Experimental studies of a wiggler-focused sheet electron beam high power millimeter-wave free-electron laser amplifier," Ph.D dissertation, Univ. of Maryland, College Park, 1995.

[25] J. H. Booske, B. D. McVey, and T. M. Antonsen, Jr., "Stability and confinement of nonrelativistic sheet electron beams with periodic cusped magnetic focusing," *J. Appl. Phys.,* vol. 73, pp. 4140–4155, 1993.

[26] M. Reiser, *Theory and Design of Charged Particle Beams.* New York: Wiley, 1994.

[27] M. A. Basten, J. H. Booske, and J. Anderson, "Magnetic quadrupole formation of elliptical sheet electron beams for high-power microwave devices," *IEEE Trans. Plasma Sci.,* vol. 22, pp. 960–966, 1994.

Shiqiu Cheng, photograph and biography not available at the time of publication.

William W. Destler (M'84–SM'90–F'92), for a photograph and biography, see this issue, p. 686.

Victor L. Granatstein (S'59–M'64–SM'86–F'92), for a photograph and biography, see this issue, p. 665.

Thomas M. Antonsen, Jr. (M'87) was born in Hackensack, NJ in 1950. He received the B.S.E.E. degree in 1973, and the M.S. and Ph.D. degrees in 1976 and 1977, all from Cornell University, Ithaca, NY.

He was a National Research Council Postdoctoral Fellow at the Naval Research Laboratory from 1976 to 1977, and a Research Scientist in the Research Laboratory of Electronics at MIT from 1977 to 1980. In 1980 he moved to the University of Maryland, College Park, where he joined the faculty of the Departments of Electrical Engineering and Physics in 1984. He has held visiting appointments at the Institute for Theoretical Physics (U.C.S.B.), the Ecole Polytechnique Federale de Lausanne, Switzerland, and the Institute de Physique Theorique, Ecole Polytechnique, Palaiseau, France. His research interests include the theory of magnetically confined plasmas, the theory and design of high power sources of coherent radiation, nonlinear dynamics in fluids, and the theory of intense laser pulses and plasmas. He is the author of over 140 journal articles and co-author of the book, *Principles of Free-Electron Lasers* (London: Chapman & Hall, 1992).

Dr. Antonsen has served on the Editorial Board of *Physical Review Letters*, *The Physics of Fluids*, and *Comment on Plasma Physics*. He was selected as a Fellow of the Division of Plasma Physics of the American Physical Society in 1986.

Baruch Levush (M'88–SM'90) received the M.Sc. degree (physics) from Latvian University in Riga in 1972 and the Ph.D. degree (physics) from Tel-Aviv University, Israel, in 1981.

In 1985 he joined the University of Maryland, College Park, where his research has focused on the physics of coherent radiation sources and the design of high-power microwave sources. In 1995 he became the Head of the Theory and Design Section of the Vacuum Electronics Branch at the Naval Research Laboratory. He is actively involved in developing theoretical models and computational tools for analyzing the operation of existing high-power microwave tubes and in inventing new concepts for high-power high-frequency coherent radiation sources. His scope of research interests is not limited to the area of coherent radiation sources. He is currently involved in research applying microwave energy for the processing of ceramic materials. In particular he is interested in modeling the heat dissipation and sintering processes in ceramic bodies subjected to microwave fields.

John Rodgers, for a biography, see this issue, p. 686.

Z. X. Zhang, photograph and biography not available at the time of publication.